Environmental Science & Technology

Article

pubs.acs.org/est

Constraints on Carbon Monoxide Emissions Based on Tall Tower Measurements in the U.S. Upper Midwest

Su Youn Kim,[†,⊥] Dylan B. Millet,[†,*] Lu Hu,[†] Michael J. Mohr,[†] Tim J. Griffis,[†] Deyong Wen,[‡] John C. Lin,[§] Scot M. Miller,[∥] and Marcos Longo[∥]

[†]University of Minnesota, St. Paul, Minnesota 55108, United States

[‡]University of Waterloo, Waterloo, ON N2L 3G1, Canada

[§]University of Utah, Salt Lake City, Utah 84112, United States

[∥]Harvard University, Cambridge, Massachusetts 02138, United States

Supporting Information

ABSTRACT: We interpret a full year of high-frequency CO measurements from a tall tower in the U.S. Upper Midwest with a time-reversed Lagrangian Particle Dispersion Model (STILT LPDM) and an Eulerian chemical transport model (GEOS-Chem CTM) to develop top-down constraints on U.S. CO sources in 2009. Our best estimate is that anthropogenic CO emissions in the U.S. Upper Midwest in 2009 were 2.9 Tg, 61% lower (a posteriori scale factor of 0.39) than our a priori prediction based on the U.S. EPA's National Emission Inventory for 2005 (NEI 2005). If the same bias applies across the contiguous U.S., the inferred CO emissions are 26 Tg/y, compared to the a priori estimate of 66 Tg/y. This discrepancy is significantly greater than would be expected based solely on emission decreases between 2005 and 2009 (EPA estimate: 23% decrease). Model transport error is an important source of uncertainty in the analysis, and we employ an ensemble of sensitivity runs using multiple meteorological data sets and model configurations to assess its impact on our results. A posteriori scale factors for the U.S. anthropogenic CO source from these sensitivity runs range from 0.22 to 0.64, corresponding to emissions of 1.6−4.8 Tg/y for the U.S. Upper Midwest and 15−42 Tg/y for the contiguous U.S. The data have limited sensitivity for constraining biomass + biofuel burning emissions and photochemical CO production from precursor organic compounds. Our finding of a NEI 2005 overestimate of CO emissions is consistent with recent assessments for individual cities and with earlier analyses based on the NEI 1999, implying the need for a better mechanism for refining such bottom-up emission estimates in response to top-down constraints.

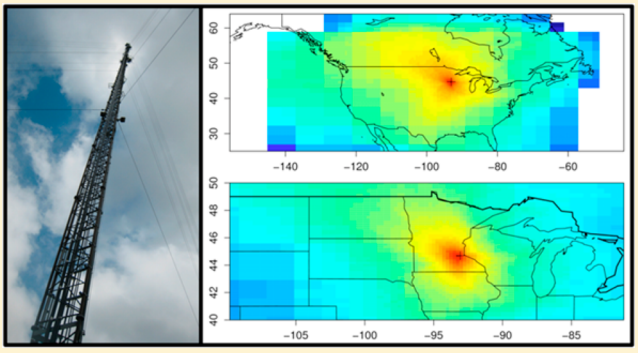

1. INTRODUCTION

Carbon monoxide (CO) is a precursor of tropospheric ozone and the dominant global sink of the hydroxyl radical (OH).[1,2] It is also widely used as a tracer for understanding sources of other atmospheric species.[3−5] Despite an expanding array of atmospheric observations, bottom-up source estimates for North America remain uncertain.[6−10] Here, we present a full annual cycle of continuous CO concentration measurements from a tall tower in the U.S. Upper Midwest, and interpret the data with a Lagrangian Particle Dispersion Model (STILT LPDM) and with an Eulerian chemical transport model (GEOS-Chem CTM) to develop new constraints on CO emissions in 2009.

CO is emitted during the combustion of biomass and fossil fuel and produced photochemically from the oxidation of methane and other volatile organic compounds (VOCs). Globally, direct emissions and secondary photochemical production are thought to be of comparable importance.[1,11] Other sources are comparatively small, and include emissions from the oceans[12] and from live and decaying plants.[13,14] The dominant loss process is oxidation by OH, and there is also a minor sink due to soil uptake.[15] The atmospheric lifetime of CO is estimated at 1−3 months.[16−18]

Within North America, anthropogenic CO emissions have been changing significantly in recent years, largely due to improved vehicle emission control systems.[19,20] Such trends augment the difficulty in accurately quantifying emissions from the bottom up. We present in this paper an analysis of CO observations from the University of Minnesota tall tower Trace Gas Observatory (KCMP tall tower), located in the Upper Midwest of the United States. The tall tower measurements provide high-resolution information with a large-scale footprint, and we employ them here in an inverse analysis to develop a

Received: March 1, 2013
Revised: July 5, 2013
Accepted: July 11, 2013
Published: July 11, 2013

   dx.doi.org/10.1021/es4009486 | Environ. Sci. Technol. 2013, 47, 8316−8324

better understanding of CO source processes in the United States for 2009. We provide top-down emission estimates for the U.S. Upper Midwest, as well as for the contiguous U.S. as a whole. The latter assume that any emission biases inferred based on our measurements manifest across the entire a priori inventory. Finally, we apply multiple transport models as well as both Lagrangian and Eulerian simulation frameworks to assess how transport uncertainties affect our top-down emission estimates.

2. METHODS

2.1. Measurements. We measure CO, H_2, and a suite of VOCs at the University of Minnesota tall tower Trace Gas Observatory (KCMP tall tower, 44.689°N, 93.073°W; 244 m height, 534 m ASL), located approximately 25 km south of Minneapolis-St. Paul, MN. Measurement details are provided in the Supporting Information (SI), and more specifics regarding the site description and sampling setup can be found in Hu et al.[3,21]

Figure 1 shows the CO mixing ratios measured at the KCMP tall tower during 2009.

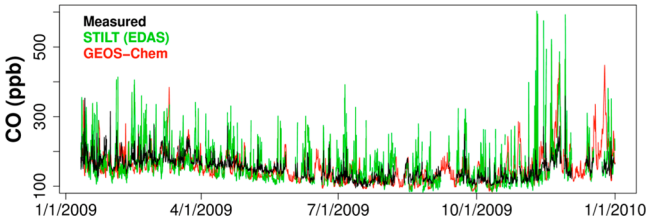

Figure 1. CO mixing ratios (2 h average) at the KCMP tall tower during 2009. Measured values (in black) are compared to those simulated by STILT (using EDAS meteorology, in green) and GEOS-Chem (at 2° × 2.5° resolution, in red).

2.2. STILT Model Description. We use the Stochastic Time-Inverted Lagrangian Transport (STILT) model[22−24] to simulate CO mixing ratios at the KCMP tall tower for 2009. STILT computes the upstream influence on a measurement site by releasing a suite of particles from the receptor and following their transport backward in time. Wind fields are provided by a mesoscale model, driven by meteorological reanalysis data, and interpolated to the explicit location of each particle. Turbulence is simulated by a Markov chain process. The evolution of particles backward in time maps the footprint function, which when coupled to a surface flux quantifies the contribution of each location in space and time to mixing ratios of an inert tracer at the receptor. Figure 2 shows the averaged footprint function at the KCMP tall tower for 2009 as derived by STILT.

For noninert tracers such as CO we must also account for the chemical evolution of particles during transport.[8] Here we apply a first-order chemical loss to the simulated CO mixing ratios based on hourly OH fields archived from a global chemical transport model simulation[25] (GEOS-Chem CTM, see below; global mean OH is 1.2×10^6 molec/cm^3). Anthropogenic CO emissions over North America are based on the EPA National Emissions Inventory (NEI)[26] for 2005. Emissions are hourly, account for variations between weekdays, Saturdays, and Sundays, and are gridded to 0.036° horizontal resolution; emission allocation is described by NOAA CSD.[27] SI Figure S1 shows our implementation of NEI 2005 for this work. Simulated emissions total 66.3 Tg/y for the contiguous U.S., and 7.45 Tg/y for the U.S. Upper Midwest (here we define the U.S. Upper Midwest as the region bounded by the western border of North and South Dakota: 104.051°W; the southern Iowa border: 40.588°N; the Canadian border; and 87°W). For comparison, the EPA NEI Emissions Trends Summary (June 2013 version) estimates total nonfire U.S. emissions at 76.7 Tg in 2005.[28] Biomass burning and biofuel emissions are taken from the Global Fire Emissions Database[29] and from Yevich and Logan,[30] respectively.

We use three meteorological data sets to drive the STILT model and to assess the impact of transport uncertainty on our analysis: EDAS (Eta Data Assimilation System) and NARR (North American Regional Reanalysis) from the National Centers for Environmental Prediction (NCEP), and BRAMS (Brazilian developments on the Regional Atmospheric Modeling System).[31−33] The horizontal domains of these three meteorological data sets are plotted in SI Figure S2. More details regarding the STILT model and the meteorological drivers used here are provided in the SI.

The STILT model was then used to simulate the CO mixing ratios at the KCMP tall tower, based on the upstream surface influence (computed using EDAS, NARR, or BRAMS meteorology) coupled with the corresponding emission rates and subsequent photochemical production and loss. Individual sources (fossil fuel combustion, biomass & biofuel burning, photochemical production, and the model boundary condition) are tracked as separate tagged tracers in the simulation, with the sum of these equal to the total ambient CO mixing ratio.

2.3. GEOS-Chem Model Description. We use the GEOS-Chem 3D CTM[25,34] to provide initial conditions, boundary conditions and CO production and loss rates for the STILT simulations. We also repeat our STILT inversion analysis using CO concentration fields from three separate GEOS-Chem simulations (carried out at 4° × 5°, 2° × 2.5°, and 0.5° × 0.667° horizontal resolution) in order to examine how our results vary with the configuration and resolution of the model used for interpretation. The 4° × 5° and 2° × 2.5° simulations were performed globally, while the 0.5° × 0.667° simulation was run over the nested domain shown in SI Figure S2 (10° to 70° N; 140° to 40°W). In all cases CO emissions over North America were implemented as described above for STILT. More model details are provided in the SI. SI Figure S3 shows boundary layer CO concentrations over North America at 0.5° × 0.667° resolution as simulated by GEOS-Chem.

3. SIMULATION AND COMPARISON WITH OBSERVATIONS

3.1. Mixing Height. The simulated tracer concentrations at the KCMP tall tower, along with any corresponding flux estimates, are directly sensitive to the model mixing height. In this section we examine the mixed layer depth and diurnal variability simulated at the KCMP receptor site using the above meteorological data sets.

Figure 3 shows the mean diurnal cycle in mixing height for each season at the KCMP tall tower based on the EDAS, BRAMS, and NARR simulations. Also shown is the mixing height from the GEOS-5 fields used to drive GEOS-Chem. As we see, the EDAS-STILT, NARR-STILT, and GEOS-Chem simulations provide a relatively consistent representation of the maximum daytime and minimum nighttime mixing depths: the difference in peak mixing height between EDAS-STILT or NARR-STILT and GEOS-Chem ranges from 68 to 220 m, whereas the mean mixing height at night (5−12 UTC; CST = UTC − 6) differs between the two STILT simulations and

dx.doi.org/10.1021/es4009486 | Environ. Sci. Technol. 2013, 47, 8316−8324

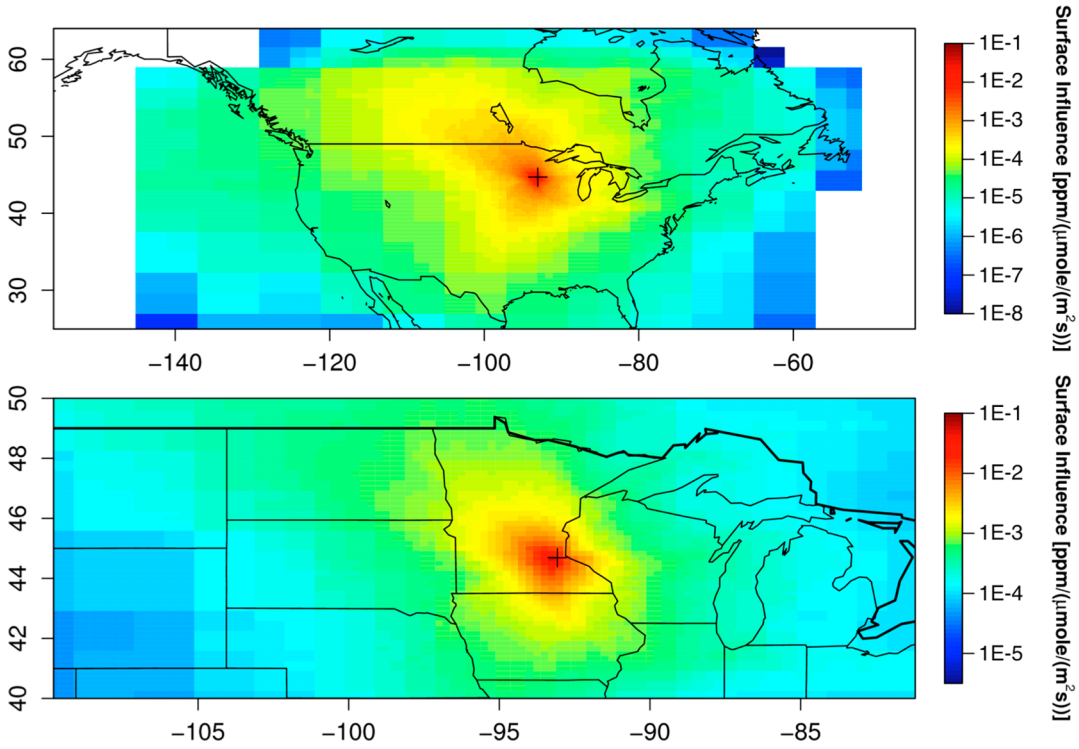

Figure 2. Average footprint function at the KCMP tall tower (indicated by the "+" symbol) for year-2009 as derived by STILT. Color scales differ between the two panels.

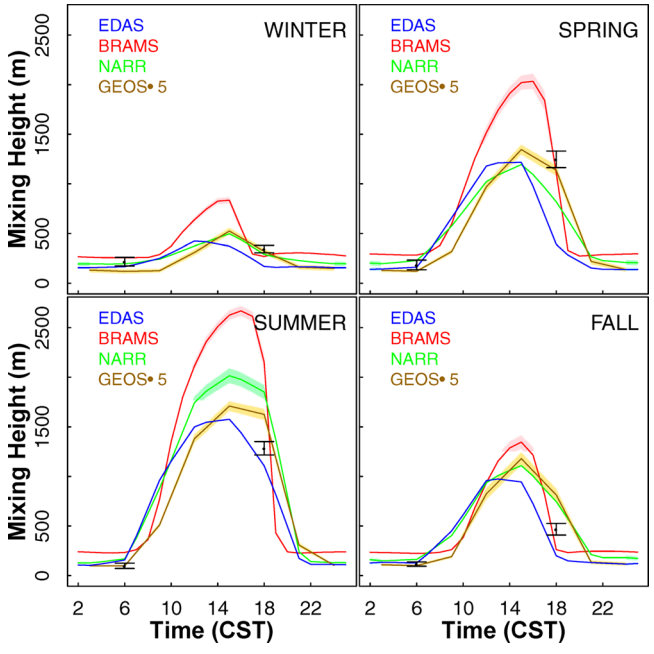

Figure 3. Mean diurnal cycle of mixing height for each season in 2009 at the KCMP tall tower. Shown are estimates from four meteorological data sets (EDAS, BRAMS, NARR, GEOS-5; colored lines) along with values inferred from nearby radiosonde observations (points). Shaded regions and error bars indicate one standard error about the mean.

GEOS-Chem by 0−108 m. On the other hand, BRAMS consistently overestimates the depth of the daytime and nighttime mixed layer relative to EDAS, NARR, and GEOS-5. Miller et al.[35] also found BRAMS mixed layer heights over the U.S. to be high compared to those from the Weather Research and Forecasting (WRF) model. We see in Figure 3 that there is some discrepancy between the simulations in terms of the timing of the growth, and especially the collapse, of the daytime mixed layer. This leads to some large relative differences at these times of day.

Figure 3 also compares the mixing heights from these various simulations with values inferred from radiosonde observations according to parcel theory.[36] The radiosondes are launched twice daily (0 UTC and 12 UTC) at Chanhassen MN, ∼25 km northwest of the tower. During spring, summer, and fall, the EDAS-STILT, NARR-STILT, and GEOS-Chem simulations are better able to capture the observed early morning (12 UTC, 6 CST) mixing height than is BRAMS-STILT. Excluding BRAMS-STILT, differences between simulated and measured mixing heights at this time range from 11 to 70 m depending on the season. The sonde measurements at 0 UTC/18 CST are more complicated to interpret because the timing corresponds closely with the evening collapse of the daytime boundary layer. Since this timing as well as the depth of the daytime mixed layer differ between the simulations, it is difficult to ascribe a discrepancy with respect to the 0 UTC radiosonde observations to one versus the other.

To further assess how uncertainty in model PBL dynamics affects our simulation and inversion results, in addition to using the separate meteorological data sets we carry out sensitivity analyses using all data, only daytime data, and only nighttime data. We also use the radiosonde-model mixing height comparisons in constructing the observational error covariance matrix for the inversion analysis described in Section 4.2.

3.2. Simulated CO Mixing Ratios. Figure 4 compares the simulated and measured 2-hourly CO mixing ratios for year-2009 at the KCMP tall tower, separated by day and night (GEOS-Chem results are shown for the 2° × 2.5° case). Here, we define daytime as 13−24 UTC (7−18 CST) and nighttime as 1−12 UTC (19−6 CST); modifying these time windows

dx.doi.org/10.1021/es4009486 | Environ. Sci. Technol. 2013, 47, 8316−8324

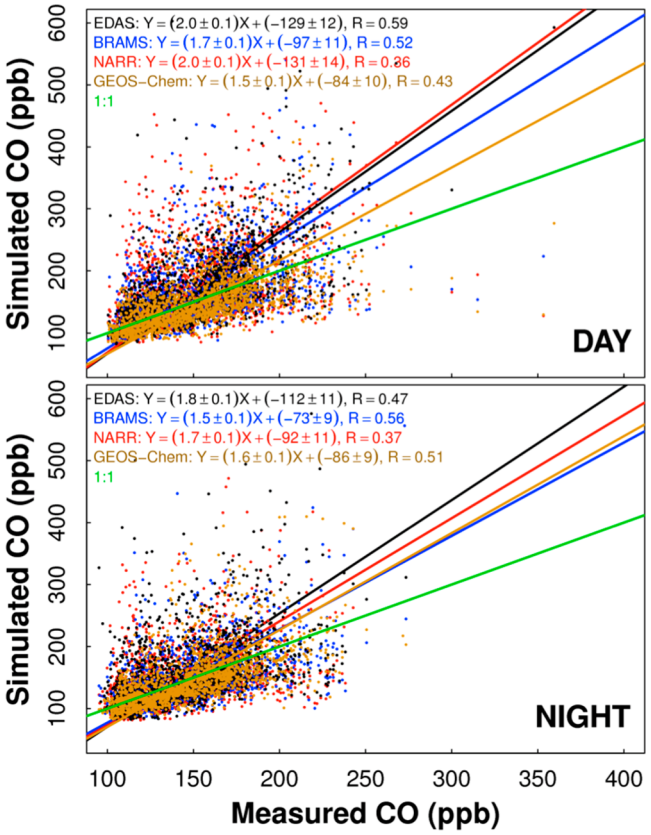

Figure 4. Comparison between simulated and measured CO mixing ratios at the KCMP tall tower during 2009. Shown are model results from STILT using the EDAS, BRAMS, and NARR meteorological fields, and from GEOS-Chem, for day (top) and night (bottom). Data shown are 2 h averages and exclude statistical outliers (>98th percentile for each month). Uncertainty values indicate 95% confidence limits.

(e.g., 16−22 UTC or 17−21 UTC for daytime) did not yield significantly different results. Only data below the monthly 98th percentile are used to avoid undue influence from statistical outliers.

Figure 4 shows some notable discrepancies between the simulated and measured CO mixing ratios. The *y*-intercepts and slopes from an orthogonal regression of the simulated versus observed mixing ratios reveal a low bias in the model background and a high bias in the model emission fluxes, respectively, compared to both the daytime and nighttime observations. Model:measurement slopes range from 1.5 (95% confidence interval: 1.44−1.56) to 2.0 (1.91−2.09) during the day and from 1.5 (1.44−1.56) to 1.8 (1.72−1.88) at night, with day-night differences likely due to diurnal changes in the accuracy of the modeled mixing height (Figure 3). All comparisons are consistent, however, in revealing a CO emission overestimate in the model.

4. CONSTRAINTS ON U.S. CO SOURCES

4.1. Bayesian Inverse Framework. We apply here a Bayesian inversion[37] to interpret the KCMP tall tower measurements in terms of quantitative constraints on U.S. sources of CO in 2009. The inverse method is a useful way to test an emission inventory constructed using a bottom-up approach, based on ambient measurements and a model simulation driven by that inventory.[8,38] Miller et al.[8] carried out an analysis of North American CO sources based on tall tower measurements in Wisconsin over several months in 2004. We build on that work here by (i) incorporating a full annual cycle of observations; (ii) employing four separate meteorological data sets (EDAS, NARR, BRAMS, GEOS-5), and both Lagrangian and Eulerian simulation frameworks, to assess the impact of transport error on the analysis; and (iii) extending the analysis to 2009 to quantify the degree to which U.S. CO emission reductions have continued in recent years.

The relationship between measured and simulated mixing ratios at our tall tower receptor site can be expressed as follows:

$$\mathbf{y} = \mathbf{K\Gamma} + \varepsilon \tag{1}$$

where $\mathbf{y}$ is the vector of measured mixing ratios, $\mathbf{\Gamma}$ is the state vector being optimized, $\mathbf{K}$ is the Jacobian matrix, defining the sensitivity of the observation variables to the state variables, and $\boldsymbol{\varepsilon}$ is the observing system error, which includes both instrumental and model contributions. In our case, the columns of $\mathbf{K}$ correspond to the tagged tracer mixing ratios for each of the source types being optimized, while $\mathbf{\Gamma}$ consists of the a posteriori scale factors for those source types.

Assuming Gaussian error distributions, the optimal solution is that which minimizes $J(\mathbf{\Gamma})$, representing the error-weighted mismatch between the modeled and measured mixing ratios, plus the error-weighted mismatch between the optimized and the a priori scale factors:

$$J(\mathbf{\Gamma}) = (\mathbf{y} - \mathbf{K\Gamma})^T \mathbf{S}_\varepsilon^{-1}(\mathbf{y} - \mathbf{K\Gamma}) + (\mathbf{\Gamma} - \mathbf{\Gamma}_a)^T \mathbf{S}_a^{-1}(\mathbf{\Gamma} - \mathbf{\Gamma}_a) \tag{2}$$

In eq 2, $\mathbf{S}_\varepsilon$ and $\mathbf{S}_a$ are the observational and a priori error covariance matrices, and each element of $\mathbf{\Gamma}_a = 1$. The solution to $\nabla_{\mathbf{\Gamma}} J(\mathbf{\Gamma}) = 0$ is then given by

$$\mathbf{\Gamma}_{post} = (\mathbf{K}^T \mathbf{S}_\varepsilon^{-1} \mathbf{K} + \mathbf{S}_a^{-1})^{-1}(\mathbf{K}^T \mathbf{S}_\varepsilon^{-1} \mathbf{y} + \mathbf{S}_a^{-1} \mathbf{\Gamma}_a) \tag{3}$$

4.2. Construction of the State Vector and Error Covariance Matrices. The observational error covariance matrix includes instrumental error ($\mathbf{S}_{inst}$) along with model errors. The instrumental error variance is determined from the detection limit (0.3 ppb) and the measurement uncertainty (10% of the measured mixing ratio). Two primary sources of model error arise from (i) uncertainty in the simulated mixing height ($\mathbf{S}_{mh}$), and (ii) from the use of a finite number of particles in the trajectory calculations ($\mathbf{S}_{particle}$). These two uncertainties are related to the surface fluxes, so we estimate each based on a relative error applied to the CO signal associated with fossil fuel, biomass burning, and biofuel emissions. For $\mathbf{S}_{particle}$ we employ a relative error of 0.13, following earlier work.[8,22] We estimate $\mathbf{S}_{mh}$ based on the radiosonde comparisons described in Section 3.1. Specifically, the relative error associated with the model mixing height is taken as the mean of $|H_{obs,i} - H_{model,i}|/H_{obs,i}$, where $H_{obs,i}$ and $H_{model,i}$ represent the observed and modeled mixing heights at time *i*. Since the first vertical level of observation in the sounding data is generally ∼280 m, we exclude mixing heights <200 m from the calculation of $\mathbf{S}_{mh}$ (these data are still included in the inversion analysis). This leads to a relative error of 0.56 for the EDAS meteorological fields, which we employ in our best-estimate optimization (see following section).

We estimate the a priori errors at 100%, based on previous assessments of bottom-up CO emission errors for North America,[7−9] and set the off-diagonal elements of $\mathbf{S}_a$ and $\mathbf{S}_\varepsilon$ to zero, so that errors are assumed to be uncorrelated. Later we

dx.doi.org/10.1021/es4009486 | Environ. Sci. Technol. 2013, 47, 8316−8324

conduct some sensitivity studies to test how our optimization results depend on the particular construction of $\mathbf{S}_\varepsilon$ and $\mathbf{S}_a$. These sensitivity runs include simulations in which $\mathbf{S}_\varepsilon$ and $\mathbf{S}_a$ are computed by maximum likelihood estimation (MLE).[39] In this case $\mathbf{S}_\varepsilon$ and $\mathbf{S}_a$ are inferred from the atmospheric data themselves, by iteratively minimizing a cost function to derive their most probable values based on the observed CO concentrations and the a priori model concentrations. The resulting diagonal elements of the covariance matrices based on MLE are 229.85 ± 5.55 ppb^2 and 0.42 ± 0.30, respectively for the EDAS-STILT simulation.

We tested several combinations of CO sources to include in the state vector for optimization. Each candidate state vector was then employed for a suite of STILT simulations using different meteorological fields (EDAS, BRAMS, and NARR) and time periods (daytime-only; nighttime-only; both) in order to assess which source combination could be resolved by the observations. We first considered a 4-element state vector, composed of scale factors for North American fossil fuel emissions, North American biomass burning + biofuel emissions, background, and photochemical production. For each of the test simulations we then calculated the averaging kernel matrix $\mathbf{A}$, quantifying the sensitivity of the retrieved emissions to their true values:

$$\mathbf{A} = \mathbf{I} - \hat{\mathbf{S}}\mathbf{S}_a^{-1} \quad (4)$$

where $\hat{\mathbf{S}}$ is the a posteriori error covariance matrix.

Results are shown in SI Figure S4 for the EDAS-STILT simulation (day + night). Averaging kernel values for the fossil fuel and background categories are >0.8, while that for biomass burning + biofuel is close to 0. There is also only weak sensitivity to the photochemical production term. Averaging kernels derived using the other meteorological data sets, and using daytime-only or nighttime-only data, exhibit the same general pattern. We therefore include North American fossil fuel emissions and the CO background as the two elements to be optimized in our state vector. Including the CO background in the state vector is also important to prevent any model bias in OH or in upwind CO sources from being aliased with a bias in domestic emissions. We further perform a sensitivity inversion using a 3-element state vector that includes North American fossil fuel emissions, the CO background, and CO photochemical production, to test for any conflation between these source categories in our baseline analysis.

For the purposes of the source inversions we define 'background CO' as that which originates outside the modeling domain (or at the termination of a back-trajectory). Since the domain varies with model configuration (as shown in SI Figure S2), the precise composition of the CO background will vary slightly as well. For instance, a model simulation over a larger domain will include some photochemically produced CO that would have occurred outside the boundary of a smaller domain, and which would in that case have been classified as "background".

4.3. CO Optimization Results. Table 1 shows the optimization results for anthropogenic CO emissions and for the CO background. Because Bayesian a posteriori error estimates can be unreliable indicators of the true uncertainty in a solution,[40−43] we instead employ a wide range of sensitivity studies designed to probe the degree of uncertainty in our findings. These include STILT simulations using EDAS, BRAMS, and NARR meteorology; daytime-only, nighttime-only and all data; a 2-element (fossil fuel, CO background) versus 3-element (fossil fuel, CO background, CO photochemical production) state vector; using varying assumptions for $\mathbf{S}_a$ and $\mathbf{S}_\varepsilon$; and inversions based on GEOS-Chem simulation results (4° × 5°, 2° × 2.5°, 0.5° × 667°). As these optimizations are done on an annual basis (i.e., the seasonality in the bottom-up inventory is treated as a hard a priori constraint), we also perform inversions using only warm-season (May−September) and only cold-season (November−February) data to test for any seasonally dependent bias, as was found previously over North America by Kopacz et al.[44] Averaging kernels for all optimization results in Table 1 are shown in SI Figure S5.

We employ as our best-estimate optimization the EDAS-STILT simulation using all data (daytime and nighttime; O1), since the EDAS mixing depths show better agreement with radiosonde observations than do the BRAMS mixing depths

Table 1. A posteriori Scale Factors for the CO Inversion, And Reduction of the Cost Function for the Best-Estimate Simulation (O1) and Various Sensitivity Studies (O2−O20)

	a posteriori scale factor			
simulation	U.S. fossil fuel	CO background	CO photochemical production	cost function reduction (%)
O1: EDAS	0.39	1.30		57
O2: EDAS, 3-element state vector	0.37	1.25	1.05	63
O3: EDAS, daytime only	0.57	1.16		45
O4: EDAS, nighttime only	0.44	1.26		48
O5: EDAS, increased $\mathbf{S}_a$[a]	0.25	1.40		70
O6: EDAS, decreased $\mathbf{S}_a$[a]	0.64	1.12		35
O7: EDAS, increased $\mathbf{S}_{mh}$[b]	0.64	1.12		35
O8: EDAS, decreased $\mathbf{S}_{mh}$[b]	0.26	1.40		69
O9: BRAMS	0.36	1.25		45
O10: NARR	0.33	1.34		60
O11: EDAS, MLE[c]	0.24	1.41		70
O12: EDAS, MLE, $\mathbf{S}_a$ + SD[d]	0.22	1.43		72
O13: EDAS, MLE, $\mathbf{S}_a$ − SD[d]	0.35	1.33		61
O14: EDAS, MLE, $\mathbf{S}_\varepsilon$ + SD[d]	0.24	1.41		70
O15: EDAS, MLE, $\mathbf{S}_\varepsilon$ − SD[d]	0.24	1.41		70
O16: EDAS, May-Sept	0.56	1.26		40
O17: EDAS, Nov-Feb	0.63	1.07		43
O18: GEOS-Chem, 4° × 5°	0.41	1.27		43
O19: GEOS-Chem, 2° × 2.5°	0.29	1.32		69
O20: GEOS-Chem, 0.5° × 0.667°	0.25	1.33		75

[a]A priori uncertainty is decreased or increased by a factor of 2. [b]Mixing height uncertainty is decreased or increased by a factor of 1.5. [c]A priori error covariance and observational error covariance are calculated by maximum likelihood estimation.[39] [d]Maximum likelihood covariance matrices are increased or decreased by their associated uncertainty.

dx.doi.org/10.1021/es4009486 | Environ. Sci. Technol. 2013, 47, 8316−8324

(Figure 3), and the simulated CO mixing ratios have higher correlation with the observations than is achieved using NARR-STILT (Figure 4). The GEOS-Chem simulations also yield high correlation with the observed mixing depths and CO concentrations, but we employ these mainly as a secondary and independent metric to evaluate the STILT results.

The KCMP tall tower observations clearly reveal an overestimate of U.S. anthropogenic CO emissions in the NEI 2005 data set. Our best-estimate a posteriori scale factor for this source is 0.39, with a range of 0.22−0.64 for the various sensitivity analyses. Our results also imply a model underestimate of the CO background as simulated by GEOS-Chem, with an a posteriori scale factor of 1.30 (1.07−1.43). An underestimate of the CO background indicates either a sink (model OH) overestimate, or else an underestimate of CO emissions upwind of the U.S.

When we perform separate optimizations for the May−September and the November−February time-frames, we do derive a slightly larger adjustment to the a priori in the warm season (scale factor of 0.56, compared to 0.63 in the cold season). However, in both cases the a posteriori result falls within the range bounded by the other (annual) sensitivity analyses, preventing us from detecting a seasonally specific bias in the prior inventory.

Figure 5 compares the CO mixing ratios measured at the KCMP tall tower with those from the best-estimate a posteriori simulation. The regression has a slope of 1.11 (1.08−1.14), a *y*-intercept of −12 ppb (−16 to −8), and a higher correlation than the a priori regression. The fact that the slope is greater than 1.0 indicates that the high bias in the model simulation is not fully removed; the optimization is constrained to a degree by the error covariance matrices $\mathbf{S}_a$ and $\mathbf{S}_\varepsilon$. Increasing the a priori error estimate, or decreasing the observational error estimate, leads to a lower scale factor for fossil fuel emissions and reduces the regression slope (e.g., O5, O8, O12; Table 1). The cost function is reduced by 57% through the best-estimate optimization, compared to 35−75% for the different sensitivity runs shown in Table 1.

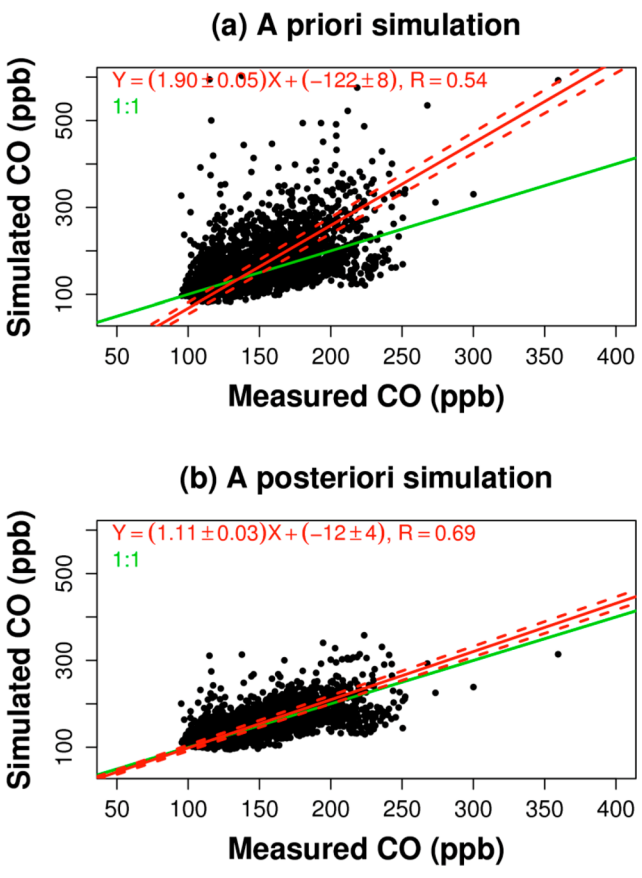

Figure 5. Linear regressions between the measured and simulated CO mixing ratios for the (a) a priori and (b) best-estimate a posteriori simulations (all data). Uncertainty values indicate 95% confidence limits.

5. CO SOURCES IN THE UNITED STATES

Our findings show that CO emissions within the KCMP tall tower footprint in 2009 are substantially overestimated using the EPA's NEI 2005. Excluding wildfires, our a priori implementation of the NEI 2005 yields anthropogenic CO emissions of 7.5 Tg for the U.S. Upper Midwest in 2005. By contrast, our best-estimate optimization indicates that anthropogenic CO emissions were only 2.9 Tg in that region during 2009, with an uncertainty range from the sensitivity runs of 1.6−4.8 Tg.

These findings are consistent with recent analyses in other regions: airborne measurements over Sacramento CA[10] and Houston, TX[6] concluded that the NEI 2005 overestimates CO emissions by 40−100% for those cities in 2009 and 2006, respectively. If our findings based on measurements in the U.S. Upper Midwest reflect a bias that manifests across the NEI inventory nationally, then the resulting flux for the contiguous United States would be 26 Tg/y, with an uncertainty range of 15−42 Tg/y.

Previous assessments of the NEI 1999 CO emissions also found evidence of a significant overestimate.[7−9,45] For example, Hudman et al.[7] applied aircraft measurements and the GEOS-Chem CTM to deduce that summertime anthropogenic CO emissions over the U.S. in 2004 were 60% lower than predicted by the NEI 1999. If the same bias were to apply year-round, the implied U.S. anthropogenic CO source would be 37 Tg/y (in 2004), 42% higher than our best estimate for 2009 of 26 Tg/y.

The most recent EPA NEI Emissions Trends Summary[28] (June 2013 version) estimates that U.S. anthropogenic nonwildfire CO emissions dropped 19% between 1999 and 2005 (from 94.4 to 76.7 Tg/y), and an additional 23% between 2005 and 2009 (to 59 Tg/y). A value of 59 Tg in 2009 is still a factor of 2 larger than our best estimate for that year of 26 Tg. The ensemble of sensitivity runs with varying meteorological inputs and error estimates result in 2009 U.S. CO emissions that are between 25% and 72% of the bottom-up EPA Emissions Trends estimate for the same year.[28]

6. DISCUSSION

We presented a full year of high-frequency CO mixing ratio measurements from a tall tower in the U.S. Upper Midwest, and applied a Lagrangian Particle Dispersion Model (STILT LPDM) and an Eulerian chemical transport model (GEOS-Chem CTM) in an inverse modeling framework to interpret the data in terms of their constraints on CO sources. We employed three separate meteorological data sets (EDAS, BRAMS, NARR) to drive STILT and to assess the impact of transport error on the simulations. Based on a seasonal and diurnal analysis of radiosonde observations near the site, and the fidelity of the various simulations in capturing the observed

dx.doi.org/10.1021/es4009486 | Environ. Sci. Technol. 2013, 47, 8316−8324

variability in atmospheric CO concentrations, we selected the EDAS fields for our best-estimate simulation.

An orthogonal regression of the simulated versus observed CO mixing ratios for 2009 revealed a clear high bias in the model, with slopes of 2.0 (daytime data) and 1.8 (nighttime data) for the EDAS-STILT simulation. The bias reflects an overestimate of anthropogenic CO emissions in the footprint of the KCMP tall tower, which are implemented in the model based on the U.S. EPA's National Emission Inventory for 2005 (NEI 2005).

We then carried out a Bayesian optimization to derive CO emissions for the U.S. Upper Midwest that are most consistent with our observations and with prior constraints. Our best estimate is that anthropogenic CO emissions in this region were 2.9 Tg in 2009. A suite of sensitivity inversions with varying meteorological inputs and error estimates give a range of 1.6−4.8 Tg. If these findings for the U.S. Upper Midwest reflect a consistent bias across the NEI inventory, then the resulting best-estimate anthropogenic CO flux for the contiguous U.S. is 26 Tg in 2009, with an uncertainty range of 15−42 Tg.

Our best-estimate optimization implies CO emissions in 2009 that are 61% lower than our a priori based on an implementation of NEI 2005. However, U.S. CO emissions have been decreasing significantly in recent years. For example, Warneke et al.[20] estimated that CO mixing ratios in the Los Angeles basin have been decreasing at an annual rate of about 7.5%/year. The EPA NEI 2008[46] inventory has recently been implemented in GEOS-Chem, and the corresponding year-2008 CO emissions are 5.7 Tg/y for the U.S. Upper Midwest and 48.7 Tg/y for the contiguous U.S. (SI Figure S6), ∼25% lower than the NEI 2005-based prior used here. Similarly, the U.S. EPA Emissions Trends Summary[28] estimates that anthropogenic CO emissions in the U.S. decreased by 23% between 2005 and 2009. The resulting bottom-up flux estimate for nonwildfire anthropogenic CO emissions in 2009 (59 Tg) is still outside the uncertainty range implied by our sensitivity inversions based on the tall tower measurements (15−42 Tg/y), and a factor of 2 larger than our best-estimate value.

As another point of comparison, the EDGARv4.2 inventory[47] provides global CO emission estimates at 0.1° × 0.1° resolution on a yearly basis from 1970 to 2008. These flux estimates (shown in SI Figures S7 and S8) are lower than the NEI values, and decline from 6.0 to 5.2 Tg/y (U.S. Upper Midwest) and from 52.0 to 44.9 Tg/y (contiguous U.S.) between 2005 and 2008, the latest year available.

The 2-fold discrepancy that we find relative to NEI 2005 is similar to findings for the NEI 1999 based on a range of studies.[7−9,45] The fact that the bias appears to persist in the NEI 2005 suggests the need for a better mechanism for refining these bottom-up estimates in response to atmospheric observations and the scientific literature. Pending updates to the NEI system for the forthcoming version[48] may help in addressing this.

■ ASSOCIATED CONTENT

Supporting Information

Information regarding the field measurements, STILT, and GEOS-Chem, as well as additional figures related to the model simulations, optimizations, and bottom-up CO emission estimates, are provided. This material is available free of charge via the Internet at http://pubs.acs.org.

■ AUTHOR INFORMATION

Corresponding Author

*E-mail: dbm@umn.edu.

Present Address

⊥S.Y.K.: Korea Institute of Science and Technology Evaluation and Planning, Seoul, South Korea.

Notes

The authors declare no competing financial interest.

■ ACKNOWLEDGMENTS

This work was supported by the National Science Foundation (Grant NO. 0937004) and by the Minnesota Supercomputing Institute. Thanks to Katie Travis for her work implementing NEI 2008 in GEOS-Chem. We thank Tom Nelson, Minnesota Public Radio (KCMP 89.3 FM), and the UMN biometeorology group for their help with the field measurements.

■ REFERENCES

(1) Holloway, T.; Levy, H.; Kasibhatla, P. Global distribution of carbon monoxide. *J. Geophys. Res.* **2000**, *105* (D10), 12123−12147.

(2) Lin, X.; Trainer, M.; Liu, S. C. On the nonlinearity of the tropospheric ozone production. *J. Geophys. Res.* **1988**, *93* (D12), 15879−15888.

(3) Hu, L.; Millet, D. B.; Mohr, M. J.; Wells, K. C.; Griffis, T. J.; Helmig, D. Sources and seasonality of atmospheric methanol based on tall tower measurements in the US Upper Midwest. *Atmos. Chem. Phys.* **2011**, *11* (21), 11145−11156.

(4) Palmer, P. I.; Suntharalingam, P.; Jones, D. B. A.; Jacob, D. J.; Streets, D. G.; Fu, Q. Y.; Vay, S. A.; Sachse, G. W. Using CO_2:CO correlations to improve inverse analyses of carbon fluxes. *J. Geophys. Res.* **2006**, *111*, D12318 DOI: 10.1029/2005JD006697.

(5) Parrish, D. D.; Trainer, M.; Holloway, J. S.; Yee, J. E.; Warshawsky, M. S.; Fehsenfeld, F. C.; Forbes, G. L.; Moody, J. L. Relationships between ozone and carbon monoxide at surface sites in the North Atlantic region. *J. Geophys. Res.* **1998**, *103* (D11), 13357−13376.

(6) Brioude, J.; Kim, S. W.; Angevine, W. M.; Frost, G. J.; Lee, S. H.; McKeen, S. A.; Trainer, M.; Fehsenfeld, F. C.; Holloway, J. S.; Ryerson, T. B.; Williams, E. J.; Petron, G.; Fast, J. D. Top-down estimate of anthropogenic emission inventories and their interannual variability in Houston using a mesoscale inverse modeling technique. *J. Geophys. Res.* **2011**, *116*, D20305 DOI: 10.1029/2011JD016215.

(7) Hudman, R. C.; Murray, L. T.; Jacob, D. J.; Millet, D. B.; Turquety, S.; Wu, S.; Blake, D. R.; Goldstein, A. H.; Holloway, J.; Sachse, G. W. Biogenic vs. anthropogenic sources of CO over the United States. *Geophys. Res. Lett.* **2008**, *35*, L04801 DOI: 10.1029/2007GL032393.

(8) Miller, S. M.; Matross, D. M.; Andrews, A. E.; Millet, D. B.; Longo, M.; Hirsch, A.; Gerbig, C.; Lin, J. C.; Daube, B. C.; Hudman, R.; Leite da Silva Dias, P.; Wofsy, S. C. Sources of carbon monoxide and formaldehyde in North America determined from high resolution atmospheric data. *Atmos. Chem. Phys.* **2008**, *8*, 7673−7696.

(9) Parrish, D. D. Critical evaluation of US on-road vehicle emission inventories. *Atmos. Environ.* **2006**, *40*, 2288−2300.

(10) Turnbull, J. C.; Karion, A.; Fischer, M. L.; Faloona, I.; Guilderson, T.; Lehman, S. J.; Miller, B. R.; Miller, J. B.; Montzka, S.; Sherwood, T.; Saripalli, S.; Sweeney, C.; Tans, P. P. Assessment of fossil fuel carbon dioxide and other anthropogenic trace gas emissions from airborne measurements over Sacramento, California in spring 2009. *Atmos. Chem. Phys.* **2011**, *11* (2), 705−721.

(11) Duncan, B. N.; Logan, J. A.; Bey, I.; Megretskaia, I. A.; Yantosca, R. M.; Novelli, P. C.; Jones, N. B.; Rinsland, C. P. Global budget of CO, 1988−1997: Source estimates and validation with a global model. *J. Geophys. Res.* **2007**, *112*, D22301 DOI: 10.1029/2007JD008459.

(12) Bates, T. S.; Kelly, K. C.; Johnson, J. E.; Gammon, R. H. Regional and seasonal variations in the flux of oceanic carbon

monoxide to the atmosphere. *J. Geophys. Res.* **1995**, *100* (D11), 23093−23101.
(13) Guenther, A. B.; Jiang, X.; Heald, C. L.; Sakulyanontvittaya, T.; Duhl, T.; Emmons, L. K.; Wang, X. The model of emissions of gases and aerosols from nature version 2.1 (MEGAN2.1): An extended and updated framework for modeling biogenic emissions. *Geosci. Model Dev.* **2012**, *5* (6), 1471−1492.
(14) Schade, G. W.; Crutzen, P. J. CO emissions from degrading plant matter: (II) Estimate of a global source strength. *Tellus B* **1999**, *51* (5), 909−918.
(15) Sanhueza, E.; Dong, Y.; Scharffe, D.; Lobert, J. M.; Crutzen, P. J. Carbon monoxide uptake by temperate forest soils: The effects of leaves and humus layers. *Tellus B* **1998**, *50* (1), 51−58.
(16) Akimoto, H. Global air quality and pollution. *Science* **2003**, *302* (5651), 1716−1719.
(17) Prather, M. J. Time scales in atmospheric chemistry: Theory, GWPs for CH_4 and CO, and runaway growth. *Geophys. Res. Lett.* **1996**, *23* (19), 2597−2600.
(18) Xiao, Y. P.; Jacob, D. J.; Turquety, S. Atmospheric acetylene and its relationship with CO as an indicator of air mass age. *J. Geophys. Res.* **2007**, *112*, D12305 DOI: 10.1029/2006JD008268.
(19) Bishop, G. A.; Stedman, D. H. A decade of on-road emissions measurements. *Environ. Sci. Technol.* **2008**, *42* (5), 1651−1656.
(20) Warneke, C.; de Gouw, J. A.; Holloway, J. S.; Peischl, J.; Ryerson, T. B.; Atlas, E.; Blake, D.; Trainer, M.; Parrish, D. D. Multiyear trends in volatile organic compounds in Los Angeles, California: Five decades of decreasing emissions. *J. Geophys. Res.* **2012**, *117*, D00V17 DOI: 10.1029/2012JD017899.
(21) Hu, L.; Millet, D. B.; Kim, S. Y.; Wells, K. C.; Griffis, T. J.; Fischer, E. V.; Helmig, D.; Hueber, J.; Curtis, A. J. North American acetone sources determined from tall tower measurements and inverse modeling. *Atmos. Chem. Phys.* **2013**, *13* (6), 3379−3392.
(22) Gerbig, C.; Lin, J. C.; Wofsy, S. C.; Daube, B. C.; Andrews, A. E.; Stephens, B. B.; Bakwin, P. S.; Grainger, C. A. Toward constraining regional-scale fluxes of CO_2 with atmospheric observations over a continent: 2. Analysis of COBRA data using a receptor-oriented framework. *J. Geophys. Res.* **2003**, *108* (D24), 4757 DOI: 10.1029/2003JD003770.
(23) Lin, J. C.; Gerbig, C.; Wofsy, S. C.; Andrews, A. E.; Daube, B. C.; Davis, K. J.; Grainger, C. A. A near-field tool for simulating the upstream influence of atmospheric observations: The Stochastic Time-Inverted Lagrangian Transport (STILT) model. *J. Geophys. Res.* **2003**, *108* (D16), 4493 DOI: 10.1029/2002JD003161.
(24) Lin, J. C.; Gerbig, C.; Wofsy, S. C.; Andrews, A. E.; Daube, B. C.; Grainger, C. A.; Stephens, B. B.; Bakwin, P. S.; Hollinger, D. Y. Measuring fluxes of trace gases at regional scales by Lagrangian observations: Application to the CO_2 Budget and Rectification Airborne (COBRA) study. *J. Geophys. Res.* **2004**, *109*, D15304 DOI: 10.1029/2004JD004754.
(25) Mao, J.; Jacob, D. J.; Evans, M. J.; Olson, J. R.; Ren, X.; Brune, W. H., St; Clair, J. M.; Crounse, J. D.; Spencer, K. M.; Beaver, M. R.; Wennberg, P. O.; Cubison, M. J.; Jimenez, J. L.; Fried, A.; Weibring, P.; Walega, J. G.; Hall, S. R.; Weinheimer, A. J.; Cohen, R. C.; Chen, G.; Crawford, J. H.; McNaughton, C.; Clarke, A. D.; Jaegle, L.; Fisher, J. A.; Yantosca, R. M.; Le Sager, P.; Carouge, C. Chemistry of hydrogen oxide radicals (HO_x) in the Arctic troposphere in spring. *Atmos. Chem. Phys.* **2010**, *10* (13), 5823−5838.
(26) Environmental Protection Agency (EPA) National Emission Inventory (NEI) 2005; http://www.epa.gov/ttnchie1/net/2005inventory.html.
(27) National Oceanic and Atmospheric Administration (NOAA) Chemical Sciences Division (CSD); ftp://aftp.fsl.noaa.gov/divisions/taq/emissions_data_2005/.
(28) Environmental Protection Agency (EPA) National Emissions Inventory (NEI) Air Pollutant Emissions Trends Data; http://www.epa.gov/ttnchie1/trends/, accessed June 2013.
(29) van der Werf, G. R.; Randerson, J. T.; Giglio, L.; Collatz, G. J.; Kasibhatla, P. S.; Arellano, A. F. Interannual variability in global biomass burning emissions from 1997 to 2004. *Atmos. Chem. Phys.* **2006**, *6*, 3423−3441.
(30) Yevich, R.; Logan, J. A. An assessment of biofuel use and burning of agricultural waste in the developing world. *Global Biogeochem. Cy.* **2003**, *17* (4), 1095 DOI: 10.1029/2002GB001952.
(31) Black, T. L. The new NMC mesoscale Eta model: Description and forecast examples. *Weather Forecast.* **1994**, *9* (2), 265−278.
(32) Freitas, S. R.; Longo, K. M.; Dias, M.; Chatfield, R.; Dias, P. S.; Artaxo, P.; Andreae, M. O.; Grell, G.; Rodrigues, L. F.; Fazenda, A.; Panetta, J. The coupled aerosol and tracer transport model to the Brazilian developments on the regional atmospheric modeling system (CATT-BRAMS)—Part 1: Model description and evaluation. *Atmos. Chem. Phys.* **2009**, *9* (8), 2843−2861.
(33) Mesinger, F.; DiMego, G.; Kalnay, E.; Mitchell, K.; Shafran, P. C.; Ebisuzaki, W.; Jovic, D.; Woollen, J.; Rogers, E.; Berbery, E. H.; Ek, M. B.; Fan, Y.; Grumbine, R.; Higgins, W.; Li, H.; Lin, Y.; Manikin, G.; Parrish, D.; Shi, W. North American regional reanalysis. *Bull. Am. Meteorol. Soc.* **2006**, *87* (3), 343−360.
(34) Millet, D. B.; Guenther, A.; Siegel, D. A.; Nelson, N. B.; Singh, H. B.; de Gouw, J. A.; Warneke, C.; Williams, J.; Eerdekens, G.; Sinha, V.; Karl, T.; Flocke, F.; Apel, E.; Riemer, D. D.; Palmer, P. I.; Barkley, M. Global atmospheric budget of acetaldehyde: 3D model analysis and constraints from in-situ and satellite observations. *Atmos. Chem. Phys.* **2010**, *10*, 3405−3425.
(35) Miller, S. M.; Kort, E. A.; Hirsch, A. I.; Dlugokencky, E. J.; Andrews, A. E.; Xu, X.; Tian, H.; Nehrkorn, T.; Eluszkiewicz, J.; Michalak, A. M.; Wofsy, S. C. Regional sources of nitrous oxide over the United States: Seasonal variation and spatial distribution. *J. Geophys. Res.* **2012**, *117*, D06310 DOI: 10.1029/2011JD016951.
(36) Holzworth, G. C. Estimates of mean maximum mixing depths in the contiguous United States. *Mon. Weather Rev.* **1964**, *92*, 235−242.
(37) Rodgers, C. D. *Inverse Methods for Atmospheric Sounding: Theory and Practice*; World Scientific: Singapore, 2000.
(38) Wang, Y. X. X.; McElroy, M. B.; Wang, T.; Palmer, P. I. Asian emissions of CO and NO_x: Constraints from aircraft and Chinese station data. *J. Geophys. Res.* **2004**, *109*, D24304 DOI: 10.1029/2004JD005250.
(39) Michalak, A. M.; Hirsch, A.; Bruhwiler, L.; Gurney, K. R.; Peters, W.; Tans, P. P. Maximum likelihood estimation of covariance parameters for Bayesian atmospheric trace gas surface flux inversions. *J. Geophys. Res.* **2005**, *110*, D24107 DOI: 10.1029/2005JD005970.
(40) Arellano, A. F.; Hess, P. G. Sensitivity of top-down estimates of CO sources to GCTM transport. *Geophys. Res. Lett.* **2006**, *33*, L21807 DOI: 10.1029/2006GL027371.
(41) Heald, C. L.; Jacob, D. J.; Jones, D. B. A.; Palmer, P. I.; Logan, J. A.; Streets, D. G.; Sachse, G. W.; Gille, J. C.; Hoffman, R. N.; Nehrkorn, T. Comparative inverse analysis of satellite (MOPITT) and aircraft (TRACE-P) observations to estimate Asian sources of carbon monoxide. *J. Geophys. Res.* **2004**, *109* (D23), D23306 DOI: 10.1029/2004JD005185.
(42) Kopacz, M.; Jacob, D.; Henze, D. K.; Heald, C. L.; Streets, D. G.; Zhang, Q. A comparison of analytical and adjoint Bayesian inversion methods for constraining Asian sources of CO using satellite (MOPITT) measurements of CO columns. *J. Geophys. Res.* **2009**, *114*, D04305 DOI: 10.1029/2007JD009264.
(43) Peylin, P.; Baker, D.; Sarmiento, J.; Ciais, P.; Bousquet, P. Influence of transport uncertainty on annual mean and seasonal inversions of atmospheric CO_2 data. *J. Geophys. Res.* **2002**, *107* (D19), 4385 DOI: 10.1029/2001JD000857.
(44) Kopacz, M.; Jacob, D. J.; Fisher, J. A.; Logan, J. A.; Zhang, L.; Megretskaia, I. A.; Yantosca, B. M.; Singh, K.; Henze, D. K.; Burrows, J. P.; Buchwitz, M.; Khlystova, I.; McMillan, W. W.; Gille, J. C.; Edwards, D. P.; Eldering, A.; Thouret, V.; Nedelec, P. Global estimates of CO sources with high resolution by adjoint inversion of multiple satellite datasets (MOPITT, AIRS, SCIAMACHY, TES). *Atmos. Chem. Phys.* **2010**, *10*, 855−876.
(45) Warneke, C.; de Gouw, J. A.; Stohl, A.; Cooper, O. R.; Goldan, P. D.; Kuster, W. C.; Holloway, J. S.; Williams, E. J.; Lerner, B. M.; McKeen, S. A.; Trainer, M.; Fehsenfeld, F. C.; Atlas, E. L.; Donnelly, S.

G.; Stroud, V.; Lueb, A.; Kato, S. Biomass burning and anthropogenic sources of CO over New England in the summer 2004. *J. Geophys. Res.* **2006**, *111* (D23), D23S15 DOI: 10.1029/2005JD006878.
(46) Environmental Protection Agency (EPA) National Emission Inventory (NEI) 2008; http://www.epa.gov/ttnchie1/net/2008inventory.html.
(47) Emission Database for Global Atmospheric Research (EDGAR), release version 4.2.; http://edgar.jrc.ec.europa.eu.
(48) Environmental Protection Agency (EPA) National Emission Inventory (NEI) 2011; http://www.epa.gov/ttnchie1/net/2011inventory.html.